In Situ Fabrication and Graphitization of Amorphous Carbon Nanowires and Their Electrical Properties

C. H. Jin,[†] J. Y. Wang,[‡] Q. Chen,[‡] and L.-M. Peng*[,†,‡]

Beijing National Laboratory for Condensed Matter Physics, Institute of Physics, Chinese Academy of Science, P.O. Box 603, Beijing 100080, P.R. China, and Key Laboratory for the Physics and Chemistry of Nanodevices and Department of Electronics, Peking University, Beijing 100871, P.R. China

Received: December 12, 2005; In Final Form: January 26, 2006

Individual amorphous carbon nanowires (a-CNWs) were fabricated inside a transmission electron microscope (TEM) by the electron beam induced deposition (EBID) method, and the a-CNWs were graphitized in situ by introducing Fe particles into these a-CNWs and controlled movement of the Fe particles in these CNWs. Detailed structural characterizations and electrical measurements were carried out, and it was found that the current-induced movement of Fe particles has significant effects in purifying the as-fabricated a-CNW, transforming the a-CNW into a graphitized-CNW (g-CNW). Two-terminal current voltage characteristics measurements showed that the g-CNW has a very good electrical conductivity with a resistivity of about $5.3 \times 10^{-4}\ \Omega$ cm, a current carrying capacity of at least 4.35 mA, and a current density of 4.6×10^8 A/cm^2, and these values are comparable to those of multiwalled carbon nanotubes. Field emission characteristics of both a-CNWs and g-CNWs were also measured, and their respective Fowler−Nordheim plots were found to have basically a linear form.

1. Introduction

Carbon nanotubes (CNTs) are currently the focus of intense research because of their unique properties and potential applications in broad areas of science and technology.[1] Their properties such as mechanical, electrical, and thermal properties are sensitive to geometrical details, which cannot be accurately controlled and usually depend intricately on the method of CNT growth. Much attention has been devoted to produce CNTs. Arc-discharge from an anode electrode containing Fe was the first method used for producing single-walled CNTs.[2] This was followed by the laser ablation method, using an Fe-mixture carbon target[3] and chemical vapor deposition (CVD) on a substrate dispersed with Fe catalyst.[4] Despite this success, precisely controlled growth of CNTs with the desired diameter, length, and quality is not yet realized, and new synthesis methods for CNTs are still highly desirable. Alternatively tubular graphitic structures were synthesized[5] via in situ annealing of amorphous carbon nanopillar in the presence of Fe particles. In this paper we report a comprehensive investigation on the in situ fabrication and modification of carbon nanowires (CNWs) by the method of electron beam induced deposition (EBID)[6] of amorphous CNWs (a-CNWs) and controlled current-induced migration and heating of Fe particles through the as-fabricated a-CNW to form polycrystalline graphitized CNWs (g-CNWs). The structures and electrical properties of both a-CNW and g-CNW were extensively characterized in situ inside the transmission electron microscope (TEM) with use of a TEM-STM system.[7]

* To whom correspondence should be addressed. E-mail: lmpeng@pku.edu.cn.
[†] Chinese Academy of Science.
[‡] Peking University.

2. Experimental Section

Individual a-CNW was fabricated on the electrochemically etched W tip by the method of electron beam-induced deposition (EBID), using a Tecnai G20 TEM. In the TEM an electron beam was focused on the W-tip on which organic molecules (mainly hydrocarbons, which are always present in the conventional TEM) were adsorbed. As a result of complex beam-induced surface reactions, the adsorbed organic molecules dissociated into deposited amorphous carbon and volatile fragments that were pumped away. In our experiments a LaB_6 filament was used. To achieve a large growth rate, the acceleration voltage was set at its maximum value of 200 kV, and a large beam current of 7.5 μA was focused onto a small area of about 40 nm (using a large spot size of 9 or 10), and the corresponding beam current was about 6.0×10^5 A/cm^2 . The typical vacuum level of our TEM chamber is about 10^{-5} Pa. The geometry of the fabricated a-CNWs was manually controlled by the movement of the electron beam. TEM experiments and composition analysis were performed in situ inside the TEM that is equipped with an EDX attachment. A microscopically flat platinum wire was used as the counter electrode to form an electrical loop, and some MWCNTs encapsulated with Fe particles were preassembled onto the platinum wire and were later used as the source of Fe for subsequent graphitization of the a-CNWs. Electrical measurements were also carried out in situ inside the TEM, using a Nanofactory TEM-STM holder at room temperature. In a typical two-terminal $I-V$ measurement, the sample was first swept under a large bias voltage to improve the electrical contact qualities at the CNW−electrode interfaces. $I-V$ characteristics of the CNWs were recorded only after the current became stable. In electrical breakdown experiments, to obtain more information on the breakdown process, the acquisition time for each $I-V$ curve with 1000 data points was set to be 50 ms. The upper current limit of our system is 4.35 mA, and the voltage limit is 140 V. To compare the field emission

10.1021/jp057240r CCC: $33.50
Published on Web 02/28/2006

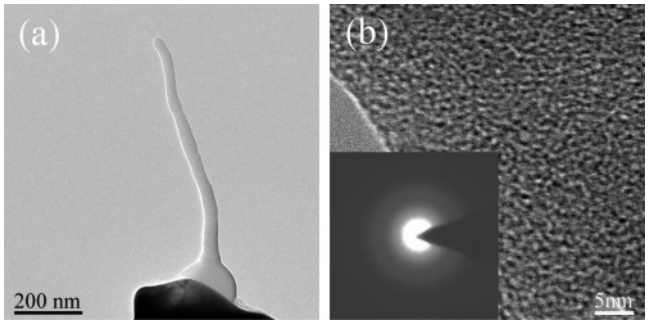

Figure 1. (a) A low magnification TEM image of a single a-CNW deposited on a W tip, with an average diameter of 29 nm and length 711 nm; (b) a HRTEM image of the a-CNW revealing its amorphous nature. The insert is a SAED pattern.

properties of the same CNW before and after graphitization accurately, the same electrode spacing was used. In all electrical measurements the electron beam was blanked whenever it was unnecessary.

3. In Situ Fabrication and Modification of a-CNWs

Shown in Figure 1a is a TEM image of an a-CNW deposited on a clean W tip. This a-CNW has an average diameter of about 29 nm and a length of about 711 nm. The growth rate for this a-CNW was estimated to be 140 nm/min. To stabilize the contact between the a-CNW and the W tip, more than enough amorphous carbon was deposited at the contact. Shown in Figure 1b and its inset are a TEM image and a selected area electron diffraction (SAED) pattern obtained from this as-fabricated a-CNW, showing clearly the amorphous nature of the as-fabricated a-CNW. It should be pointed out that the a-CNW does not have a regular circular cross section. Although the averaged width of the a-CNW is about 29 nm, its thickness is different from its width and is determined by the deposition time employed in the fabrication process. The width/thickness ratio of the as-fabricated a-CNW was determined by tilting the a-CNW along its long axis, and it was found that this ratio is about 0.85 for the typical fabrication conditions.

To modify the structure and electrical property of the as-fabricated a-CNW, it was moved toward and made contact with a multiwalled CNT (MWCNT) that was filled with Fe[8] (Figure 2a). This MWCNT and some other MWCNTs encapsulated with Fe particles were assembled onto the top Pt electrode (not shown in this figure, but in Figure 6) prior to our in situ experiments. It was reported recently by Regan et al.[9] and Svensson et al.[10] that mass transport along a CNT may be controlled by the current through it via the electromigration mechanism.[11] Experimentally it was found that the direction of the movement of the Fe particles encapsulated within the CNTs is consistent with that of the electron flow, i.e., opposite to the current. By applying a negative voltage on the top Pt electrode we obtained an electron flow from the CNT to the a-CNW. When the current exceeded a threshold value the encapsulated Fe particles in the CNT started to move toward the a-CNW as shown in Figure 2b. After almost all encapsulated Fe particles in the CNT had been moved to the a-CNW (Figure 2b), the empty CNT was moved away and a new CNT containing more Fe particles was brought in and more Fe particles were transferred into the a-CNW as shown in Figure 2c. The Fe particles in the a-CNW were controlled to move up and down within the a-CNW via alternating the electron current direction, and as will be shown below, the impurities in the as-fabricated a-CNW were largely removed and the CNW was transferred into partially graphitized CNW (g-CNW).

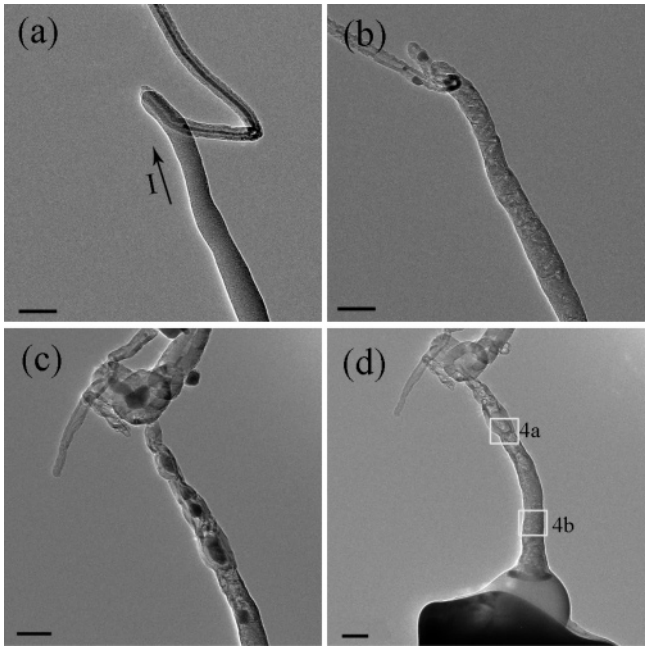

Figure 2. TEM images showing introduction of Fe particles into the a-CNW and structural modification of the a-CNW via the Fe particles. (a) The a-CNW (the lower part) was controlled to make contact with an Fe-filled MWCNT (the upper part), with the arrow indicating the direction of the current (opposite to the flow of electrons). (b) Almost all Fe particles encapsuled inside the MWCNT shown in part a had been introduced into the a-CNW. (c) Another MWCNT with more Fe particles was brought into contact with the CNW, and more Fe particles were introduced into the CNW. (d) The iron particles were moved to the bottom of the CNW by a large current (0.25 mA). Scale bar: 50 nm.

By applying a large current (~0.25 mA here) almost all Fe particles were moved to the bottom of the CNW as shown in Figure 2d. From this low magnification TEM image, some obvious morphography changes were observed on the CNWs. On introducing Fe particles into the a-CNW, the CNW was seen to have broadened having its average diameter increased from about 29 nm to 39 nm. A lot of empty space or voids were left in the g-CNW where the Fe particles were moved, making the structure somehow a CNT-like structure. It should be noted that part of the CNW was broken due to the greatly increased current in introducing Fe particles into the CNW, the whole length of the CNW decreased to about 445 nm. In principle this effect could be avoided by using a smaller current or an alternative method for supplying Fe particles, such as the method of thermal evaporation.

4. Structural Characterization

The composition of the CNW was analyzed in the TEM with X-ray energy-dispersive spectroscopy (EDX), and the results shown in Figure 3, parts a, b, and c, were obtained respectively from the as-fabricated a-CNW, during the modification of the CNW via the introduction and movement of the Fe particles, and after the modification. Figure 3a shows that the as-fabricated a-CNW was composed mainly of carbon (~97%), but characteristic peaks for O, Si, and Pt also appeared in the EDX spectrum. The Pt signal appeared because we used a Pt electrode in our experiments, while the Si signal appeared mainly because of the Si EDX detector and the relatively large counts we used in our experiments. The as-fabricated a-CNW might contain a certain amount of hydrogen due to the hydrocarbon precursors involved in the deposition of amorphous carbon, but the signals

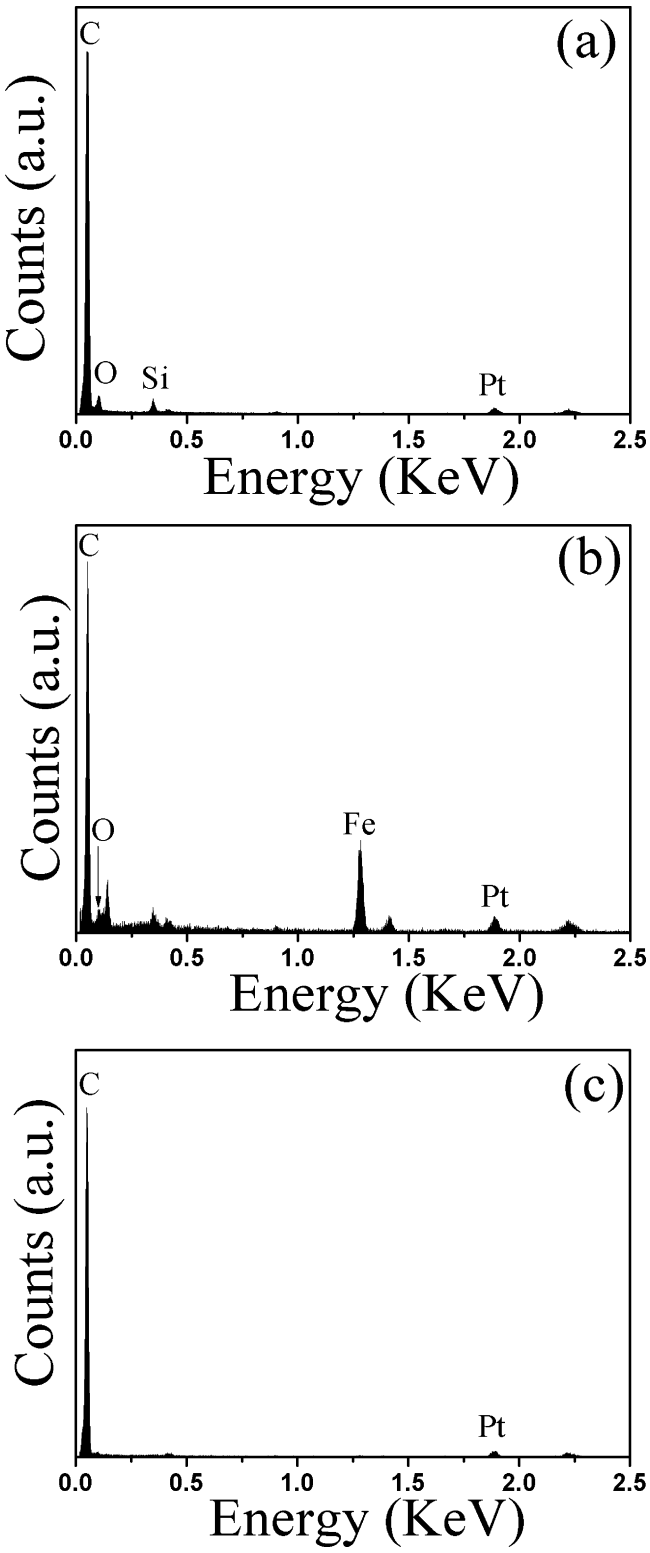

Figure 3. EDX spectra recorded from (a) a freshly fabricated a-CNW, (b) when the CNW was modified via Fe particles, and (c) after the modification and all Fe particles were moved toward the bottom of the CNW.

for hydrogen could not be identified by our EDX spectrometer. Figure 3b shows a strong Fe peak, since Fe particles were introduced onto the as-fabricated a-CNW. After the modification of the a-CNW, the Fe particles were moved away from the main part of the CNW, and the corresponding EDX spectrum shown in Figure 3c recorded from the top region of the CNW shows a very clean and simple composition of the modified CNW. The characteristic C peak dominates the spectrum, and the finite

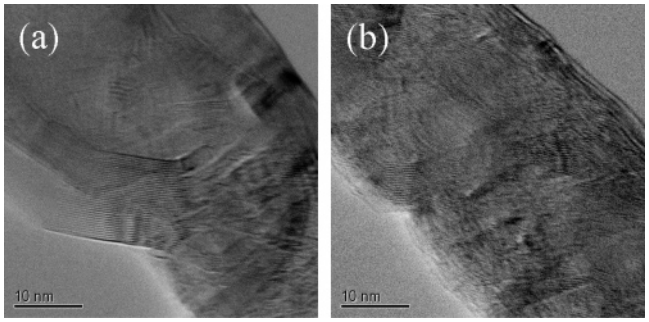

Figure 4. Two high-resolution TEM images taken from different parts of the CNW as marked in Figure 2d.

O peak observed in Figure 3a disappeared. The residual O in the as-fabricated a-CNW might have reacted with the Fe particles and been carried away from the CNW together with the Fe particles after the modification of the CNW.

Apart from its composition change, the as-fabricated a-CNW was also largely graphitized during the modification process in which Fe particles were controlled to move up and down along the CNW. Shown in Figure 4a,b are two high-resolution TEM (HRTEM) images, showing different parts of the modified g-CNW along the g-CNW as marked in Figure 2d. These HRTEM images clearly show the existence of layer structures with a spacing of ~0.34 nm, which is consistent with the interlayer spacing of graphite sheets.

It is well established that Fe particles may act as catalyst in the growth of CNTs, especially in the CVD growth of CNTs.[12] The growth process is often described as C segregation and emergence of layered carbon structures from the super-saturation of the C-metal solution under a high temperature in the presence of a flow of hydrocarbons and metal catalyst nanoparticles. A molten or partially molten Fe particle is usually required for these processes. In our experiments the temperature of the Fe particles was partially raised by current-induced Joule heating. With use of a reasonable thermal conductivity value of 50 Wm^{-1} K^{-1} for graphite,[13] a simple heat transfer analysis suggests that the "hottest" temperature should be around 540 K, which occurs at the middle of the g-CNW. But this temperature is very low compared with the equilibrium eutectic temperature of the corresponding Fe−C alloy of about 1150 °C. Although the melting point of nanometer-sized particles could be much lower than that of the bulk material,[14] the diameter of the Fe particles introduced into the CNW is about 30 nm, which is far too larger to have any significant size effect on their melting temperature. Electron collisions with the Fe particles in the CNW may result in large momentum transfer, which could have a profound effect when the electron current density is high. Experimentally it was found that the movement of the Fe particles exhibited liquid-like behavior with good fluidity, but TEM observations revealed that these Fe particles remained mostly round and corresponding SAED patterns recorded during the movement of the Fe particles show that long-range ordering existed while these particles were moving. The Fe particles were neither solid nor liquid, and could best be referred as in a quasisolid state.[15] Recently it was found that CNTs may be formed by diffusion of C atoms through the sp^2 bonded C cap on the iron catalyst.[16] The observed change of morphography of the CNW shown in Figure 2d could thus be explained as due to the Fe−C interactions. The increase in the diameter of the CNW is due to the segregation of C atoms from the side-surface of the Fe particle. An inhomogeneous distribution of C density and diameter along the CNW axis may result from the fluctuation in the movement speed and direction of the Fe particles. In general a lower speed causes more C

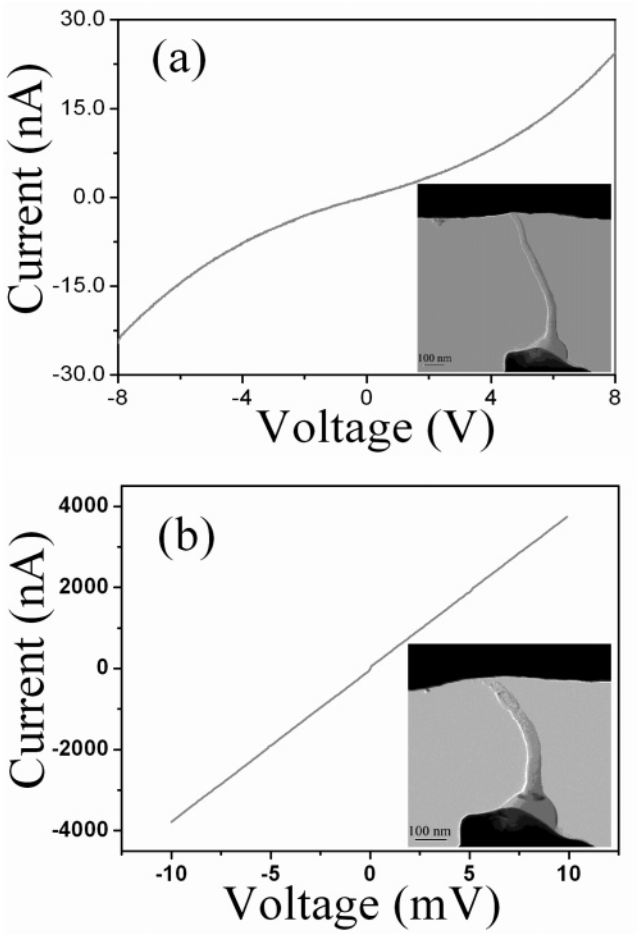

Figure 5. *I*−*V* curves recorded for the same carbon nanowire (a) before and (b) after graphitization. The inserts are corresponding TEM images.

atoms to segregate out of the Fe particle leading to a larger diameter of the g-CNW. When the movement of the Fe particles was stopped in the CNW for a few seconds, carbon atoms would be nearly homogeneously segregated surrounding the Fe particles, forming closed structures that look like graphite cages with Fe particles encapsulated inside it. In general these graphite sheets were not well oriented as shown in Figure 4b, which resulted from the wavy traces left behind by the Fe particles along the CNW. Some amorphous carbon could still exist in the CNWs which remained outside the traces of the Fe particles or had not enough time to react with the Fe particles. Thus the resultant CNW is more like a polycrystalline graphite CNW, i.e., g-CNW.

5. Electrical Characterization

5.1. Two-Terminal *I*−*V* Characteristics. Figure 5a shows the two-terminal *I*−*V* characteristics of the as-fabricated a-CNW (inset), and Figure 5b shows that for the same CNW but modified by the Fe particles (inset). For the a-CNW (Figure 5a) the *I*−*V* curve is nonlinear, and a very small current of about 25 nA was obtained when a large bias 8.0 V was applied. Electrical transport in amorphous carbon is conventionally attributed to the hopping mechanism where tunneling transitions between localized states occur and the energy difference between the initial and final states is bridged by the electron−phonon scattering process.[17] The estimated resistance from the linear part of the *I*−*V* curve (Figure 5a) around zero voltage is about 633 MΩ, corresponds to an electrical resistivity of about 68.9 Ω cm, and this value is similar to the lower value reported for amorphous carbon,[18] and the resistivity is known to be sensitive to several parameters such as hydrogen content, deposition temperature, and also the doping that may have resulted from the oxygen as shown in the EDX spectra of Figure 3.

After graphitization the electrical conductivity of the modified g-CNWs was significantly improved as evidenced in the *I*−*V* curve shown in Figure 5b. The linear nature of the *I*−*V* curve suggests that good ohmic contacts with both metal electrodes had been made to the g-CNW, and the electrical current reached up to 3.8 μA under a small bias voltage of 10 mV. The total electrical resistance as derived from the linear *I*−*V* curve of Figure 5b for the g-CNW is 2.6 kΩ, which corresponds to an electrical resistivity about 5.2×10^{-4} Ω cm that is a little larger but still comparable to that of in-plane electrical resistivity of graphite.[18] This may result from following reasons: (1) the contact resistance that cannot be excluded from the two-terminal *I*−*V* measurementand (2) the interlayer conductance involved in the transport process since the graphitic sheets in the g-CNW were not perfectly aligned. The significant increase in the electrical conductance of the g-CNW compared to that of the a-CNW is mainly due to the much improved alignment of the π-bonds nearest-neighbor sp^2 hybrids.

5.2. Current Carrying Capacity. The current carrying capacity of the CNW is a key parameter that would determine whether the CNW could be used in nanoelectronic circuits, as for example interconnects. Here the current carrying capacity and electrical breakdown behavior of the a-CNWs and g-CNWs were tested. Shown in Figure 6a,b are two *I*−*V* curves recorded respectively for an a-CNW and a g-CNW. For the a-CNWs, it was found that they have a relatively poor current sustainability. Figure 6a shows that the breakdown occurred within 50 μs (which is the time interval we used for recording the data) when the voltage reached a threshold value at 9.6 V. The current immediately before the breakdown was 1.1 μA, corresponding to a current density of about 2.2×10^5 A/cm^2. This value is even lower than that of the electromigration threshold for conventional metallization lines in microelectronic circuits. Shown in Figure 6c,d are TEM images before and after the a-CNW was broken. The original continuous a-CNW is found to break into two separate parts, and the failure region became thinner compared to others parts of the a-CNW as a result of the current-induced displacement of atoms in a typical electromigration process. When the a-CNW was modified into a g-CNW, Figure 6b shows that its current capacity was increased to at least 4.35 mA, and the later value corresponds to a current density of 4.6×10^8 A/cm^2, which is comparable to that reported for a MWCNT,[19] and is among the highest current densities tolerable by any conductor at room temperature. At low bias an ohmic behavior is observed. However, at about 0.25 V the *I*−*V* curve changed showing a super-linear increasing conductance with increasing bias. Similar *I*−*V* behavior has been reported for MWCNTs where it was attributed to the intershell tunneling induced conductance increase. In our case it might result from the anticipation of multishells of the polycrystalline graphite CNW in the conductance (see Figure 4) and the thermal dependence of resistance for graphite since the electrical resistance of the graphite drops with increasing temperature.[20] Such high current sustainability for g-CNWs may originate from the combined networks of sp^2 and sp^3 bonds.

5.3. Electron Field Emission. The electron field emission properties of the a-CNWs and g-CNWs were measured in situ with the W tip as the cathode and the Pt electrode as the anode. Shown in parts a and b of Figure 7 are the recorded electron field emission current versus voltage curves for the same CNW

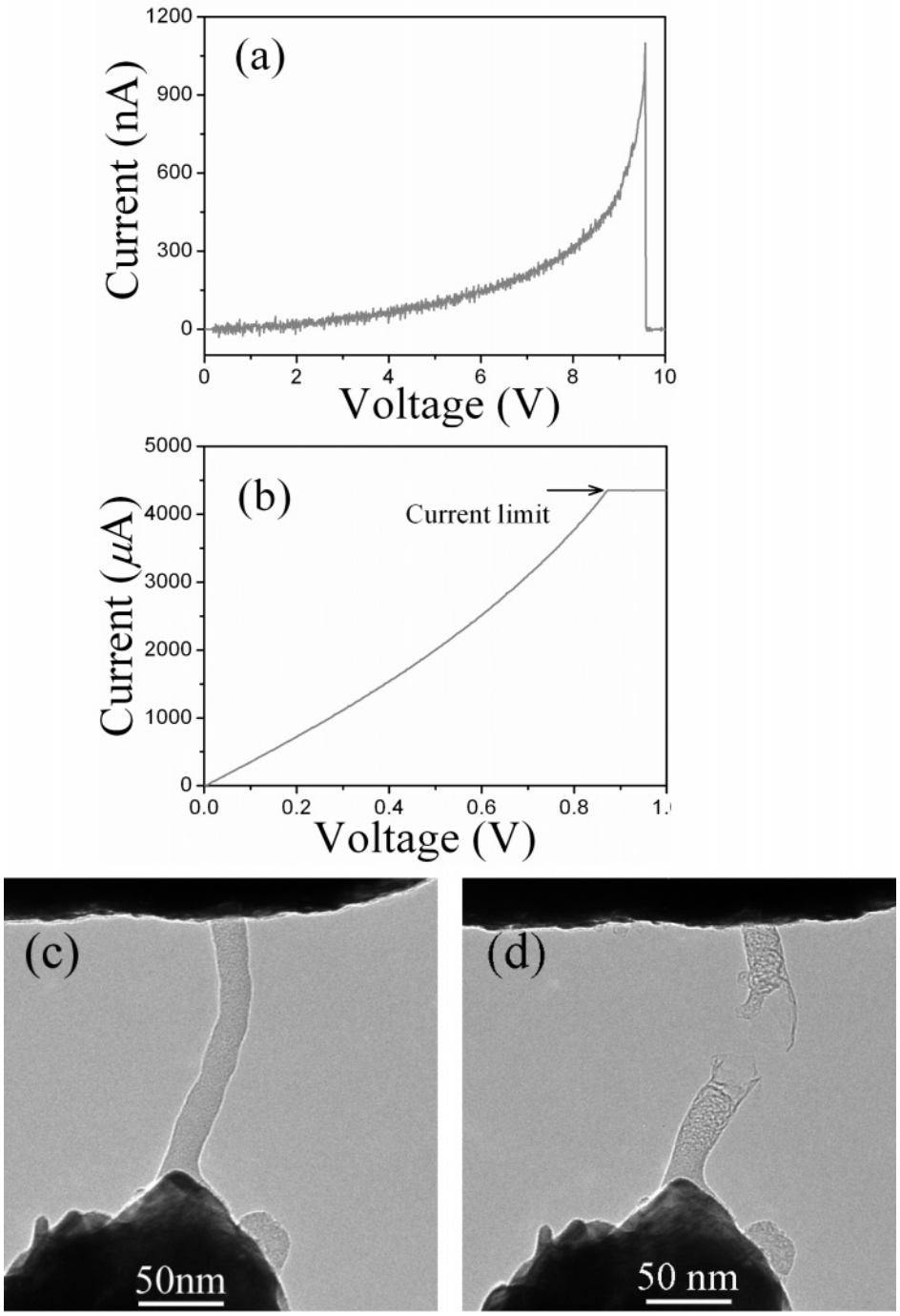

Figure 6. Current carrying capacity measurements for the (a) a-CNWs and (b) g-CNWs, repectively, and TEM images (c) before and (d) after the a-CNW was broken down.

before and after graphitization, respectively. Usually the Fowler−Nordheim (FN) law[21] is used to analyze the field emission $I-V$ measurements, which gives a relationship between the electron emission current and the local field at the emitter surface

$$I = A\frac{1.5 \times 10^{-6}}{\phi}\left(\frac{V}{d}\right)^2 \gamma^2 \exp\left(\frac{10.4}{\sqrt{\phi}}\right) \exp\left(-\frac{(6.44 \times 10^9)\phi^{1.5} d}{\gamma V}\right) \quad (1)$$

where A is the effective emission area, ϕ is the work function of the emitter, d is the distance between the electrodes, and γ is the so-called field enhancement factor.

The conventional way to determine A and γ from the measurements is to make a FN plot, i.e., to plot $\ln(I/V^2)$ versus $1/V$, and eq 1 predicts that this plot should appear as a straight line with its slope depending on d, ϕ, and γ. Experimentally d can be directly determined from TEM imaging, γ can then be obtained by taking a reasonable value for ϕ (e.g., 5 eV[22] for carbon-based emitters). Insets in Figure 7a,b show that the FN plots for both the a-CNW and g-CNW may be fitted well with straight lines, indicating that the electron field emission from both the a-CNWs and g-CNWs follows roughly the F−N law. Listed in Table 1 are relevant parameters associated with the electron field emission from the a-CNW and g-CNW. The relative smaller aspect ratio for the g-CNW used here (only 12) is unfavorable for enhancing the local electric field at the emitting tip, making it a less favorable electron field emitter when compared with that of a CNT both in its turn-on voltage and maximum emission current density.[23] We expect, however,

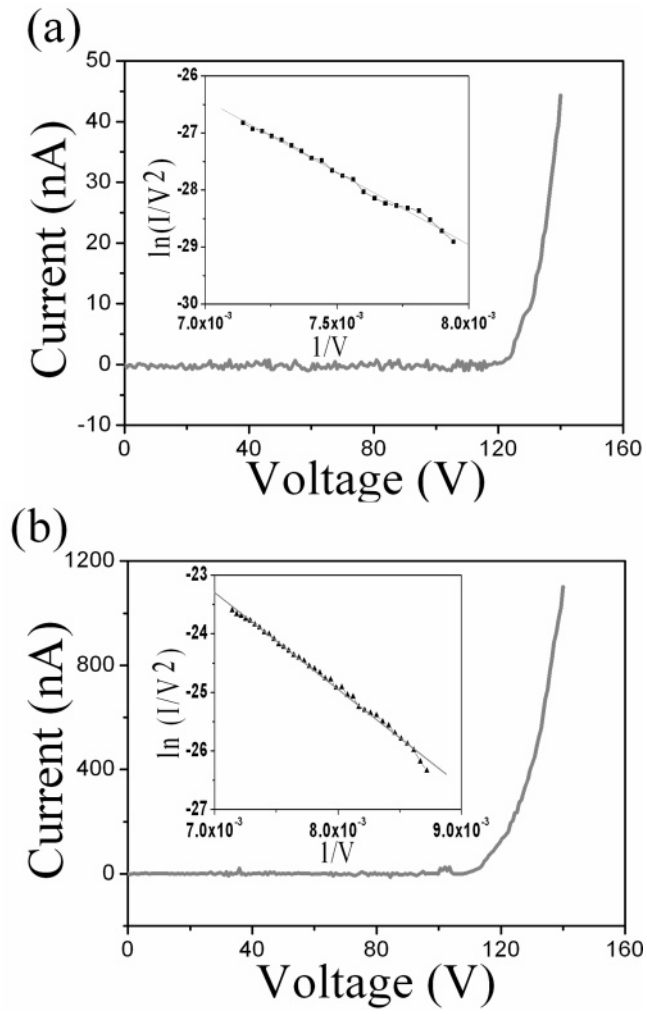

Figure 7. Electron field emission current−voltage characteristics for the same CNW (a) before and (b) after graphitization. The insets are corresponding *F*−*N* plots. The electrode distance was set to the same value of 1.48 μm.

TABLE 1: Relevant Field Emission Parameters Extracted for the a-CNW and g-CNW[a]

	a-CNW	g-CNW
turn-on voltage[b] (V)	130.5	110.6
max current (nA)	44.3	1101
max current density (A/cm^2)	7.3×10^3	1×10^5
field enhancement factor γ	42	65
effective emission area (m^2)	7.2×10^{-15}	1.3×10^{-16}

[a] The electrode spacing during field emission measurement was 1.48 μm. [b] Defined as the voltage required for extracting 10 nA current from the emitter.

that the stability of the g-CNW might be better and a g-CNW with a larger aspect ratio will have a better field emission performance.

6. Conclusions

In summary, CNWs were fabricated, modified, and comprehensively characterized. It was shown that an a-CNW may be transformed into a g-CNW via the introduction into and controlled movement of Fe particles in the a-CNW. In situ electrical transport measurements show that the g-CNWs have a very good current carrying capacity that is at least 4.6×10^8 A/cm^2, and a low electrical resistivity of about 5.3×10^{-4} Ω cm, making the g-CNW a good candidate for nanoelectronics applications.

Acknowledgment. This work was supported by the Ministry of Science and Technology (973 Grant No. 001CB610502, 863 Grant No. 2004AA302G11), National Science Foundation of China (Grant No. 10434010), the Ministry of Education (Grant Nos. 10401 and 20030001071), and the National Center for Nanoscience and Technology of China. We thank Mr. J. Su for providing the CNT samples.

References and Notes

(1) Dekker, C. *Phys. Today*. **1999**, *52*, 22−28.

(2) Iijima, S.; Ichihashi, T. *Nature* **1993**, *363*, 603−605.

(3) Thess, A.; Lee, R.; Nikolaev, P.; Dai, H. J.; Petit, P.; Robert, J.; Xu, C. H.; Lee, Y. H.; Kim, S. G.; Rinzler, A. G.; Colbert, D. T.; Scuseria, G. E.; Tomanek, D.; Fischer, J. E.; Smalley, R. E. *Science* **1996**, *273*, 483−487.

(4) Igarashi, S.; Korbori, K.; Shiraishi, M.; Kroto, H. W. *J. Phys. Chem. Solids* **1993**, *54*, 1841−1848.

(5) Ichihashi, T.; Fujita, J.; Ishida, M.; Ochiai, Y. *Phys. Rev. Lett*. **2004**, *92*, 215702.

(6) Hans Koops, W. P.; Kretz, J.; Rudilph, M.; Weber, M.; Dahm, G.; Lee, K. L. *Jpn. J. Appl. Phys*. **1994**, *33*, 7099−7107.

(7) Jin, C. H.; Wang, J. Y.; Wang, M. S.; Su, J.; Peng, L.-M. *Carbon* **2005**, 43, 1026−1031.

(8) Che, R. C.; Peng, L.-M.; Chen, Q.; Duan, X. F.; Zou, B. S.; Gu, Z. N. *Chem. Phys. Lett*. **2005**, *375*, 59.

(9) Regan, B. C.; Aloni, S.; Ritchie, R. O.; Dahmen, U.; Zettl, A. *Naure* **2004**, *428*, 924−927.

(10) Svensson, K.; Olin, H.; Olsson, E. *Phys. Rev. Lett*. **2004**, *93*, 145901.

(11) Sorbello, R. S. *Solid State Phys.* **1998**, *51*, 159−231.

(12) Dresselhaus, M. S.; Dresselhaus, G.; Avouris, Ph. *Carbon Nanotubes*; Ascheron, C. E., Kolsch, H. J., Skolaut, W. Eds.; Springer: Berlin, Germany, 2001; pp 29−52.

(13) Kelly, B. T. *Physics of Graphite*; Applied Science Publisher: London, UK, 1981; pp 222−251.

(14) Thomson, W. *Philos. Mag*. **1871**, *42*, 448.

(15) Iijima, S.; Ichihashi, T. *Phys. Rev. Lett*. **1986**, *56*, 616−619.

(16) Raty, J.-Y.; Gygi, F.; Galli, G. *Phys. Rev. Lett*. **2005**, *95*, 096103.

(17) Mott, S. N. *Conduction in Non-crystalline Materials*; Clarendon Press: Oxford, UK, 1987.

(18) *Properties of Amorphous Carbon*; Ravi, S., Silva, P., Eds.; Inspec: London, UK, 2003; pp 209−216.

(19) Bourlon, B.; Glattli, D. C.; Placais, B.; Berroir, J. M.; Miko, C.; Forro, L.; Bachtold, A. *Phys. Rev. Lett*. **2004**, *92*, 026804.

(20) Tyler, W. W.; Wilson, A. C. *Phys. Rev*. **1953**, *89*, 870−875.

(21) Brodie, I.; Spindt, C. A. Vacuum microelectronics. In *Advances in Electronics and Electron Physics*; Hawkes, V P. W., Ed.; Academic Press: New York, 1992; Vol. 83, pp 1−106.

(22) Nilsson, L.; Groeing, O.; Groening, P.; Kuettel, O.; Schlapbach, L. *J. Appl. Phys*. **2001**, *90*, 768−780.

(23) Bonard, J. M.; Kind, H.; Stockli, T.; Nilssion, L. *Solid-State Electron*. **2001**, *45*, 893−914.